LAWRENCE
LIVERMORE
NATIONAL
LABORATORY

LLNL-JRNL-666536

# Adiabat-Shaping in Indirect Drive Inertial Confinement Fusion

K. L. Baker, H. F. Robey, J. L. Milovich, O. S. Jones, V. A. Smalyuk, D. T. Casey, A. G. MacPhee, A. Pak, P. M. Celliers, D. S. Clark, T. D. Doppner, O. L. Landen, J. L. Peterson, L. F. Berzak-Hopkins, C. R. Weber, S. W. Haan, S. Dixit, E. Giraldez, A. V. Hamza, K. S. Jancaitis, J. J. Kroll, K. N. Lafortune, B. J. MacGowan, J. D. Moody, A. Nikroo, C. C Widmayer

January 26, 2015

Physics of Plasmas

## Disclaimer

# Adiabat-Shaping in Indirect Drive Inertial Confinement Fusion

K.L. Baker, H.F. Robey, J.L. Milovich, O.S. Jones, V.A. Smalyuk, D.T. Casey, A.G. MacPhee, A. Pak, P.M. Celliers, D.S. Clark, T. D. Döppner, O.L. Landen, J.L. Peterson, L.F. Berzak-Hopkins, C.R. Weber, S.W. Haan, S. Dixit, E. Giraldez, A.V. Hamza, K.S. Jancaitis, J.J. Kroll, K.N. Lafortune, B.J. MacGowan, , J.D. Moody, A. Nikroo, C.C Widmayer

**Abstract**

Adiabat-shaping techniques were investigated in indirect drive inertial confinement fusion experiments on the National Ignition Facility as a means to improve implosion stability while still maintaining a low adiabat in the fuel. Adiabat-shaping was accomplished in these indirect drive experiments by altering the ratio of the picket and trough energies in the laser pulse shape, thus driving a decaying first shock in the ablator. This decaying first shock is designed to place the ablation front on a high adiabat while keeping the fuel on a low adiabat. These experiments were conducted using the keyhole experimental platform for both three and four shock laser pulses. This platform enabled direct measurement of the shock velocities driven in the glow-discharge polymer (GDP) capsule and in the liquid deuterium, the surrogate fuel for a DT ignition target. The measured shock velocities and radiation drive histories are compared to previous three and four shock laser pulses. This comparison indicates that in the case of adiabat-

shaping the ablation front is initially driven by a high shock velocity, and therefore a high shock pressure and adiabat. The shock then decays as it travels through the ablator to pressures similar to the original low-adiabat pulses when it reaches the fuel. This approach takes advantage of initial high ablation velocity, that favors stability, and high-compression, that favors high stagnation pressures.

## I. Introduction

Initial experiments conducted on the National Ignition Facility focused on laser pulse shapes that launched four shocks, designed to drive the fuel at a low adiabat, and allow the fuel to undergo a high compression ratio necessary for ignition. These experiments, however, only achieved a modest neutron yield of ~$5x10^{14}$ neutrons. A recent assessment of these shots (T Ma, 2013) showed experimental evidence that at the higher peak drive conditions these implosions had a high degree of ablator mix into the DT fuel, compromising implosion performance (M. J. Edwards, 2013). In this paper, the original four-shock laser pulse shape will be referred to as the low foot, LF. Recent gains of an order-of-magnitude in neutron production have been demonstrated by the use of a three shock laser pulse consisting of ~ 3x higher picket energy as compared to the low foot pulse with little experimental evidence of ablator mix. (O. A. Hurricane, 2014) (H.-S. Park, 2014) This approach has shown significant $\alpha$-particle self-heating (Brian Spears, 2012) that had not been seen in inertial confinement fusion experiments prior to this NIF campaign. In this paper, the laser pulse shape used for this latter campaign will be referred to as the high foot, HF. The increased energy in the foot, picket plus trough, of the HF pulse provides for larger ablation velocities at the ablation front, predicted in simulations (V.

Goncharov and O. A. Hurricane, 2012) and in experiments (D. T. Casey, 2014) (K. S. Raman, 2014) to alter the phase of the RM oscillations and hence to reduce the growth rate of these hydrodynamic instabilities. The HF pulse as it has been implemented thus far, however, leaves the fuel on a high adiabat making it more difficult to achieve the high fuel compression ratio needed to achieve ignition.

In direct drive inertial confinement fusion, adiabat-shaping has been predicted in theory and in simulations to make direct drive capsule implosions more stable. (V. N. Goncharov, 2003) At least two methods have been investigated for adiabat-shaping in direct drive targets; the decaying shock method (V. N. Goncharov, 2003)(Anderson, 2003) and the relaxation method (R. Betti, 2005). In the direct drive decaying-shock method of adiabat-shaping a strong first shock is driven which then decays as it travels through the capsule shell. In the relaxation method, a small picket is used in front of the main pulse with a temporal gap between the two to enable the capsule shell to relax before the main pulse drives the capsule. Both of these methods are used to increase the stability of the capsule implosion by enabling the ablator to be at a higher adiabat, for increased stability, and the fuel to maintain a low adiabat for higher fuel compression. Direct drive experiments have indeed shown that both approaches to adiabat-shaping can decrease the growth of lower order laser imprinting in planar targets. (V. A. Smalyuk, 2007)

While demonstrated in direct drive, there was skepticism in the community as to whether adiabat-shaping (AS) techniques could be applied to indirect drive inertial confinement fusion due to the time response of the hohlraum radiation temperature used to drive the implosion. Simulations of indirect-drive adiabat-shaping in hohlraums, however, indicated that it was indeed feasible. (J. L. Milovich, 2014) (J. L. Peterson L. F., 2014) These simulations predicted that decaying first shock pulses provide more stable implosions, similar to the HF pulse shape,

and still achieve a low adiabat in the fuel, enabling a higher fuel compression ratio similar to the LF pulse shape. Capsule simulations looking specifically at the effects of hydrodynamic instability with changes to the foot of the laser pulse shape have shown that the strength of the first shock plays an important role in determining Richtmyer-Meshkov (RM) (Richtmyer, 1960) (Meshkov, 1969) oscillations on the ablation front. (J. L. Peterson, 2014) These surface oscillations can couple to the capsule interior through subsequent shocks before experiencing Rayleigh-Taylor (RT) growth. (Rayleigh, 1900) (Taylor) By altering the phase of the RM oscillations at the ablation front, the total hydrodynamic growth for adiabat-shaped pulses can be lower than the LF pulse even though the inner adiabat is similar. More recent capsule simulations scanning the space of foot and trough drive levels have found that the picket strength mainly sets the outer ablator adiabat while the trough level primarily sets the inner ablator and fuel adiabat. (D. S. Clark, 2014) In this paper, we take the first step in testing these predictions experimentally by presenting the measured shock velocity and hohlraum radiation temperature history for both three and four shock adiabat-shaped pulses in a keyhole experimental platform and compare them with their non-adiabat shaped counterparts. The shock velocity in the capsule and in the liquid deuterium can then be directly related to the shock pressure via the Hugoniot relationship and hence enables a direct estimate of the capsule and fuel adiabat and the expected benefits of stability at the ablation front and compression ratio of the fuel. In addition previous hydrodynamic growth instability post-shot analyses have strongly indicated that calibrating to accurate VISAR data is essential for having a predictive model of instability growth. (K. S. Raman, 2014) These VISAR measurements, therefore, are essential for interpretation and modelling of hydrodynamic instability experiments using these pulse shapes.

**Experimental Results**

Each of the adiabat-shaped keyhole experiments described in this article used targets consisting of a gold-walled hohlraum (9.43 mm in length, 5.75 mm in diameter with a 3.1 mm diameter laser-entrance-hole) as shown in the inset of Fig. 1a. A cone protruding through the side of the hohlraum and into the capsule enables the measurement of the shocks driven both in the capsule and in the liquid deuterium filling the capsule and the cone. (H. F. Robey, 2012) The capsule itself is a polystyrene (CH) capsule (nominal outer radius of 1108 μm and a thickness of 195 μm) doped with 1-2 atomic % silicon to reduce x-ray preheat of the fuel. The liquid deuterium inside the capsule and cone is maintained at a temperature of 21.5 K and provides a validated surrogate (H. F. Robey, 2012) (H. F. Robey P. M.-S., 2014) for the shock propagation in an ignition experiment that would utilize a DT ice layer.

The shocks are driven by temporally shaped laser pulses, which are incident on the walls of the hohlraum, where they are converted primarily to thermal x rays. A small portion of this x-ray radiation is then incident on the capsule that subsequently ablates the surface and drives spherical shocks into the capsule and fuel when the hohlraum is properly tuned. The entire shape of the five laser pulses discussed in this article are shown in Fig. 1a, and for clarity Fig. 1b shows just the foot, picket and trough, for each of the pulses. These include the LF pulse, dashed black curve in Fig 1, designed to drive four shocks with a low fuel adiabat, which was the primary pulse used in the initial experiments on the NIF National Ignition Campaign (NIC). This laser pulse consists of four plateaus or levels which are used to create the four shocks launched during the implosion. The HF pulse, shown by the red dashed line in Fig. 1, has three levels. As can be easily seen, the HF pulse has a much higher picket and trough energy and power than the LF pulse promoting greater stability at the ablation front.(V. Goncharov and O. A. Hurricane,

2012)(D. T. Casey, 2014) Capsule implosions driven by the HF pulse, however, have a higher fuel adiabat, making it more difficult to achieve a high fuel compression ratio for the available laser energy. To take advantage of both, the LF pulse, promoting low fuel adiabat and the potential for a high fuel compression ratio, and the HF pulse, producing larger ablation front velocities and scale-lengths and consequently more stable implosion, three new laser pulse shapes were designed and tested. The first pulse shape was a four-shock variation on the low foot pulse, which we will refer to as the first low-foot adiabat-shaped pulse or AS LF 1. The AS LF 1 pulse shape is shown as the purple line in Fig. 1 and differs from the LF pulse, the black line, primarily by the increased energy in the picket, 23 kJ vs 15 kJ for the LF. The second pulse shape was another four-shock variation on the low foot pulse, which we will refer to as the second low-foot adiabat-shaped pulse or AS LF 2. The AS LF 2 pulse shape is shown as the blue line in Fig. 1 and differs from the AS LF 1 pulse, the purple line, by a further increase in the picket energy, 30 kJ vs 23 kJ, and by a decrease in the trough power, 1 TW vs. 1.5 TW in the LF and AS LF 1 pulse shapes. This AS LF 2 variant was proposed to encourage further stability, higher picket energy, while still keeping the fuel adiabat as low as possible (Clark 2014). The third adiabat-shaped pulse was a three-shock variation of the HF pulse shape that we will refer to as the high-foot adiabat-shaped pulse or HF AS. The HF AS pulse shape is shown as the green line in Fig. 1 and has the same picket energy as the HF pulse shape, 38 kJ, while the trough power level has been reduced from 4 TW to 1 TW, for the same reason as for the AS LF 2, to reduce the fuel adiabat. The change in the second level power, from 42 TW to 35 TW, was introduced to minimize swings in the implosion symmetry predicted by our HYDRA (Marinak 2001) integrated hohlraum simulations. The timing of all subsequent pulses was appropriately

adjusted to achieve the desired shock merger; approximately 5 microns below the initial ice-gas interface in a corresponding DT layered target.

The variations in the pulse shapes between the adiabat-shaped pulses and their LF and HF counterparts, shown in Fig. 1, lead to variations in the hohlraum drive. The hohlraum drive in each of these experiments was measured with the Dante diagnostic. This instrument is a set of filter and mirror combinations of 18 x-ray diodes (Kline, et al., 2010) (DeWald, et al., 2004). The collected signals from these 18 channels can be analyzed to obtain the spectrally resolved x-ray power radiated from the hohlraum walls .The x-ray temperature unfolds for each of the five laser pulse shapes are shown in Fig. 2. The same color convention as used in Figure 1 is used throughout this paper. The HF pulse, represented by the red dashed-line, has the highest overall x-ray radiation temperature during the picket and trough part of the laser pulse. As can be seen in Fig 2, both the HF and the LF, black dashed-line, pulses, produce an increasing radiation temperature during the trough portion of the laser pulse before the launch of the second shock. In contrast, all three of the adiabat-shaped pulses have a decreasing temperature in time during this period. The radiation temperature produced by all three adiabat-shaped pulses in the picket, 119 eV for AS LF 1, 120 eV for AS LF 2 and 113 eV for AS HF, is close to that of the HF pulse, 122 eV. However, by the time when the second level of the laser pulse is incident on the hohraum wall the radiation temperature inside the hohlraum for the three adiabat-shaped pulses, 92 eV for AS LF 1, 92 eV for AS LF 2 and 90 eV for HF AS, has dropped to a value very close to that of the one obtained from the LF pulse, ~87 eV, and much further away from the temperature in the HF pulse hohlraum, ~115 eV. Looking specifically at the radiation temperature produced by the AS LF 1 pulse, we see that the hohlraum radiation temperature decays from 1.1 ns < $t$ < 5.15 ns and can be fit to a power law of the form $T_r = 114.5t^{-0.18}$. As

determined from the spectral unfolds of the Dante diagnostic, all pulse shapes produced similar x-ray fractions of M-band energy, defined as the hohlraum x-ray emission for energies greater than 1.8 keV, as the HF and LF shots, between 10 to 13% at peak drive

The temporal radiation flux produced by these laser pulses drives shocks in the capsule and in the liquid deuterium fuel surrogate. The shock velocities and merger times were measured in the experiments reported here, on both the equator and pole of the capsule using the NIF velocity interferometer system for any reflector, VISAR, diagnostic. (P. M. Celliers, 2004) (Hollenbach, 1972) The VISAR laser illuminates the liquid deuterium and capsule with a red-light laser beam, at 659.5 nm. Once the shock pressure becomes high enough(>~0.5 Mbar), the shock-front becomes reflective and Doppler shifts the laser light. (P. M. Celliers G. C., 2000) This Doppler shifted light is collected and sent through an interferometer where one of the two legs introduces a time delay. The resulting interferogram represents the interference of the Doppler shifted light from the shock at two different times, with the time delay chosen to achieve the desired phase shift for a given shock strength. Unfolding the interferogram enables the determination of the shock velocity history. Figure 3a shows the shock front velocity time histories corresponding to the five pulses described above, along the equator of the capsule, again using the same color convention as in Figures 1 & 2. In these VISAR traces, the beginning of the trace represents the shock velocity of the first shock as it traverses the capsule. A jump in the velocity is observed as the first shock leaves the ablator and enters the liquid deuterium. A subsequent jump in velocity occurs when the second shock merges with the first shock and again when the third shock merges with the combined two shocks, etc. The VISAR traces disappear when the shock velocity exceeds ~150 km/sec, the point at which self-blanking occurs in liquid deuterium. As indicated

by the DANTE diagnostic, showing the radiation temperature increasing through the trough region for both LF and HF pulses, the VISAR diagnostic also shows a slow increase in the first-shock velocities during the same period. This is indicated by the shaded regions in Fig 3 for both LF and HF pulses. In contrast the three adiabat-shaping pulses have a decaying first shock as the first shock approaches the ablator/liquid deuterium interface and a steady first-shock velocity through the liquid deuterium before merging with the second shock (also indicated by the appropriate shaded regions). It is worth noticing that the first shock velocity at the inner surface of the ablator before break-out into the liquid deuterium for the three adiabat-shaped pulses is very similar to the LF pulse, ~15 km/sec. In particular the first shock velocity for AS LF 1 was 16 km/sec, AS LF 2 was 17.5 km/sec and HF AS was 18 km/sec. In contrast the HF pulse produces a first shock velocity at the inner surface of the ablator of ~23 km/sec.

Post shot simulations of the experiments were performed using the HYDRA code. (M. M. Marinak, 2001). The code was used to compare the shock velocities from the simulations with the unfolded shock velocities measured in the experiments. The simulated shock velocities are shown as dotted lines on Fig. 3a for each of the laser pulses. The simulated shock velocities are not subject to blanking, an absorption of the probe laser due to electron-hole pairs created in the GDP capsule from absorbed M-band x rays or hot electrons. Therefore the simulated velocities appear at the onset of the shock propagating in the shell with experimental data beginning after the shock has propagated some distance in the GDP shell. The ablation pressure in the capsule can be approximated as the hohlraum flux, $\sigma T_r^4$, multiplied by (1- the CH albedo) ~ $T_r^{-0.3}t^{-0.1}$ (K. Eidmann, 1995) and divided by the exhaust velocity of partially ionized CH, $\sim T_r^{0.55}$ (N. B. Meezan, 2013). Hence $P_A$, ~ $T_r^{3.15}t^{-0.1}$. From CH Hugoniot measurements in the 1.5-5 Mbar regime, (M. A. Barrios, 2012) $P_A \sim v_s^{2.2}$, hence $v_s \sim T_r^{1.43}$. This scaling can be used to compare

the ratio of the simulated shock velocity as the shock enters the ablator with the measured shock velocity just before the shock leaves the ablator and enters the liquid deuterium and the measured hohlraum radiation temperatures at these two times for each of the five laser pulses. The results of this comparison are listed in Table 1 with the agreement for all five pulses within 6%. Using the measured time dependence of the decay of the radiation temperature between the picket and the trough of $T_r \alpha t^{-0.18}$ a very simplistic model would suggest that the shock velocity would decay as $v_s \alpha t^{-0.3}$. A fit to this analytical estimate, $v_s = 28.6t^{-0.3}$ km/s, is also included in Fig. 3a, purple circles, showing good agreement with the simulated and measured shock velocity time dependence for the AS LF 1 pulse shape. It should be noted that using this simple model to look at the temporal decay of the shock does not include important effects such as the relative distance between the ablation front and the shock front as a function of time and the propagation time of the ablation front pressure to the shock front as the ablation pressure/velocity is decaying in time. Fig. 3b represents a HYDRA simulation of a keyhole experiment, and it shows the position of the leading shock as a function of time in red. This leading shock position represents the surface from which the VISAR is reflected. Horizontal dashed lines indicate the radial locations of the ablator-D2 interface and the radius at which a DT ice / DT gas interface would be located in the corresponding ignition target.

Simulations were also used to predict the expected performance of these laser pulse shapes in a DT ignition experiment and predict the fuel adiabats. Figure 4 shows the simulated pressure of the leading shock front as a function of position in the ablator. This shows that in both the LF, dashed black line, and the HF, dashed red line, the shock pressure is increasing as the first shock reaches the ablator-fuel interface in contrast to the three adiabat-shaping pulse shapes where the pressure is decreasing the entire time the first shock traverses the ablator. The HYDRA code was

also used to predict the fuel adiabat based on the results from the keyhole measurements. The fuel adiabat, $\alpha$, is defined as $\alpha = P/P_{cold}$, where $P$ is the mass averaged DT fuel pressure at peak velocity, and $P_{cold}$ is the minimum pressure at 1000 gcm$^{-3}$ which is very close to the ideal Fermi degenerate pressure for DT.(S. W. Haan, 2011) The simulation results of the fuel adiabat as a function of time, Fig. 5a, indicated that the high foot has the highest fuel adiabat at 2.3 (specifically defined at the time of peak fuel velocity), the AS HF pulse is slightly lower at 2.1, the two AS LF pulses with varying picket energy have the next highest fuel adiabat at ~1.6 to 1.7 and the low foot pulse has the lowest fuel adiabat at ~1.5. To address the question as to which shock most strongly affects the fuel adiabat, the adiabat was quantified as the average over the central 20% of the fuel layer in Fig. 5b. This has the feature of clearly indicating the separate contributions of the various shocks to the adiabat. For the HF, for example, the contributions of the 1st and 2nd shocks to the adiabat are 1.55 and 1.8, respectively. The 3rd is very small, and not clearly seen. The AS HF, by comparison, shows a reduced 1st shock contribution of 1.4 but an increased 2nd shock contribution of 1.75, and a minor 3rd shock contribution. This shows that the final fuel adiabat is most strongly affected by the first shock strength in the fuel for both the three and four shock pulse shapes. In the three shock adiabat-shaped pulse, however, the contributions to the fuel adiabat from the first and second shocks are nearly equal.

The experimental shock velocities in the GDP and liquid deuterium can be used to reaffirm equation of state models for the two materials and can be combined with equation of state models for DD and DT developed by Kerley (Kerley, 2004) to enable a comparison with the simulated adiabats resulting from the first shock velocities presented above. In particular Fig. 6 shows the shock velocity from the first shock as it travels from the GDP ablator into the liquid deuterium plotted as a function of shock velocity in the GDP vs. shock velocity in the liquid

deuterium. The experimental data points for each of the five laser pulse shapes are listed along with the release curve using the GDP(LEOS 5400) (Sebastien Hamel, 2012) and liquid deuterium (LEOS 1014), the latter of which is based on the Kerley model. (Kerley, 2004) The experimental measurements all agree within the error bars of the shock velocity measurements, $\pm$2%, with the equation of state tables for GDP and liquid deuterium. The adiabat driven by the first shock can be estimated from the measured shock velocities in liquid deuterium in combination with Kerley's equation of state models for DD and DT. The equation of state model can be used to generate the Hugoniot for liquid deuterium from its initial cryogenic state, 0.17 g/cm$^3$ at 21.5 K. (Souers, 1986) The measured shock velocities for each of the five laser pulses can then be used in conjunction with the equation of state model to predict the pressure in the liquid deuterium(or DT ice) driven by the first shock. An isentrope is then generated beginning at that pressure and density point on the Hugoniot as shown in Fig. 7. The Hugoniot and the isentropes for each of the five laser pulses along with the cold curve are shown in Figure 7 a and b. Figure 7b shows a more limited pressure-density region where the adiabat is determined. The adiabat in this case is then defined as the ratio of the pressure along the isentrope at the density of 125 g/cm$^3$ to the pressure of the cold curve at that same density for each of the five laser pulse shapes. Table 2 shows the experimental velocities measured in the GDP and liquid deuterium for each of the five laser pulses along with the inferred pressure using Kerley's model, the calculated adiabat using the data and the model and the simulated adiabat values from the first shock. The agreement is within 2.4% for the LF and the two AS LF laser pulse shapes. The largest discrepancy in the adiabat between the experimental data coupled with the model and the simulations is for the AS HF which is still within 8%.

## II. Conclusions

Adiabat-shaping for the indirect-drive ignition program has been demonstrated with both 3 and 4 shock pulses. For each of the adiabat-shaped pulses, the DANTE diagnostic measured a decaying radiation temperature profile in the hohlraum during the trough, and the VISAR directly measured the decaying first shock in the GDP shell and in the liquid deuterium. The first shock velocity measured at the GDP/$D_2$ interface was significantly lower than the HF laser pulse shape but higher than the LF pulse shape. The two 4-shock adiabat shaped pulses had measured shock velocities at the interface between the shell and the liquid deuterium that were very similar to the low foot pulse shape, ~15 km/sec, and a predicted fuel adiabat that was only slightly higher that the low foot, 1.6 to 1.7 vs. the low foot's 1.5. The shock velocity of the three shock adiabat shaped pulse was significantly higher than the low foot but its fuel adiabat was in between the low foot and the high foot at 2.1. Adiabat-shaping shots had similar fractions of M-band energy as the HF and LF shots, between 10 to 13%. These pulses will be further tested in layered DT capsules to further verify the implosion performance.

We thank K. S. Raman for useful discussions and a careful reading of the manuscript. This work was performed under the auspices of the U.S. Department of Energy by LLNL under Contract DE-AC52-07NA27344.

# REFERENCES


1) T. Ma et al., "Onset of Hydrodynamic Mix in High-Velocity, Highly Compressed Inertial Confinement Fusion Implosions," Phys. Rev. Lett. **111**, 085004 (2013).

2) M. J. Edwards, P. K. Patel, J. D. Lindl, L. J. Atherton, S. H. Glenzer et al., "Progress towards ignition on the National Ignition Facility," Phys. Plasmas **20**, 070501 (2013).

3) O. A. Hurricane et al., "Fuel gain exceeding unity in an inertially confined fusion implosion," Nature **506**, 343 (2014).

4) H.-S. Park et al., "High-Adiabat High-Foot Inertial Confinement Fusion Implosion Experiments on the National Ignition Facility" Phys. Rev. Lett. **112**, 055001 (2014).

5) V. Goncharov and O. A. Hurricane, LLNL Report No. LLNL-TR-562104, 2012; LLNL Report No. LLNLTR-570412, 2012.

6) Brian Spears, D.S. Clark, M.J. Edwards, S.W. Haan, J.D. Lindl, D.H. Munro, L.J. Suter, C.A. Thomas, "Alpha heating and implosion performance in cryogenic layered NIF implosions,"

Bull. Am. Phys. Soc. **57**, GO4.00005 (2012).

7) D. T. Casey et al., "Reduced instability growth with high-adiabat high-foot implosions at the National Ignition Facility," Phys. Rev. E, **90**, 011102-1 (2014).

8) K. S. Raman, V. A. Smalyuk, D. T. Casey, S. W. Haan, D. E. Hoover, O. A. Hurricane, J. J. Kroll, A. Nikroo, J. L. Peterson, B. A. Remington, H. F. Robey, D. S. Clark, B. A. Hammel, O. L. Landen, M. M. Marinak, D. H. Munro, K. J. Peterson, and J. Salmonson, "An in-flight radiography platform to measure hydrodynamic instability growth in inertial confinement fusion capsules at the National Ignition Facility," Phys. Plasmas **21**, 072710 (2014).

9) V. N. Goncharov, J. P. Knauer, P. W. McKenty, P. B. Radha, T. C. Sangster, S. Skupsky, R. Betti, R. L. McCrory, and D. D. Meyerhofer, "Improved performance of direct-drive inertial confinement fusion target designs with adiabat shaping using an intensity picket," Physics of Plasmas **10**, 1906 (2003).

10) K. Anderson and R. Betti, "Theory of laser-induced adiabat shaping in inertial fusion implosions: The decaying Shock," Physics of Plasmas **10**, 4448 (2003).

11) R. Betti, K. Anderson, J. Knauer, T. J. B. Collins, R. L. McCrory, P. W. McKenty, and S. Skupsky, "Theory of laser-induced adiabat shaping in inertial fusion implosions: The relaxation Method," Physics of Plasmas **12**, 042703 (2005).

12) V. A. Smalyuk, V. N. Goncharov, K. S. Anderson, R. Betti, R. S. Craxton, J. A. Delettrez, D. D. Meyerhofer, S. P. Regan, and T. C. Sangster, "Measurements of the effects of the intensity pickets on laser imprinting for direct-drive, adiabat-shaping designs on OMEGA," Physics of Plasmas 14, 032702 (2007).

13) H. F. Robey, P. M. Celliers, J. L. Kline, A. J. Mackinnon, T. R. Boehly, O. L. Landen, J. H. Eggert, D. Hicks, S. Le Pape, D. R. Farley, M.W. Bowers, K. G. Krauter, D. H. Munro, O. S. Jones, J. L. Milovich, D. Clark, B. K. Spears, R. P. J. Town, S.W. Haan, S. Dixit, M. B. Schneider, E. L. Dewald, K. Widmann, J. D. Moody, T. D. Döppner, H. B. Radousky, A. Nikroo, J. J. Kroll, A.V. Hamza, J. B. Horner, S. D. Bhandarkar, E. Dzenitis, E. Alger, E. Giraldez, C. Castro, K. Moreno, C. Haynam, K. N. LaFortune, C. Widmayer, M. Shaw, K. Jancaitis, T. Parham, D. M. Holunga, C. F.Walters, B. Haid, T. Malsbury, D. Trummer, K. R. Coffee, B. Burr, L.V. Berzins, C. Choate, S. J. Brereton, S. Azevedo, H. Chandrasekaran, S. Glenzer, J. A. Caggiano, J. P. Knauer, J. A. Frenje, D. T. Casey, M. Gatu Johnson, F. H. Séguin, B. K. Young, M. J. Edwards, B. M. Van Wonterghem, J. Kilkenny, B. J. MacGowan, J.

Atherton, J. D. Lindl, D. D. Meyerhofer, and E. Moses, "Precision Shock Tuning on the National Ignition Facility," Phys. Rev. Lett. **108**, 215004 (2012)

14) H. F. Robey, P. M. Celliers, J. D. Moody, J. Sater, T. Parham, B. Kozioziemski, R. Dylla-Spears, J. S. Ross, S. LePape, J. E. Ralph, M. Hohenberger, E. L. Dewald, L. Berzak Hopkins, J. J. Kroll, B. E. Yoxall, A. V. Hamza, T. R. Boehly, A. Nikroo, O. L. Landen, and M. J. Edwards, "Shock timing measurements and analysis in deuterium-tritium-ice layered capsule implosions on NIF**,"** Physics of Plasmas **21**, 022703 (2014).

15) J. L. Milovich et al., "Design of indirectly-driven, high-compression ICF implosions with improved hydrodynamic stability," to be submitted to Physics of Plasmas.

16) J. L. Peterson, L. F. Berzak Hopkins, O. S. Jones and D. S. Clark "Differential ablator-fuel adiabat tuning in indirect-drive implosions" submitted to Phys. Rev. Lett. (2014)

17) J. L. Peterson, D. S. Clark, L. P. Masse, and L. J. Suter, "The effects of early time laser drive on hydrodynamic instability growth in National Ignition Facility implosions," Physics of Plasmas **21**, 092710 (2014).

18) R. D. Richtmyer, Commun. Pure Appl. Math. **13**, 297 (1960).

19) E. E. Meshkov, Izv. Acad. Sci. USSR Fluid Dynamics **4**, 101 (1969).

20) Lord Rayleigh, Scientific Papers II (Cambridge, England, 1900).

21) G.I. Taylor, Proc. R. Soc. London, Ser. A **201**, 192 (1950).

22) D. S. Clark, D. C. Eder, S. W. Haan, D. E. Hinkel, O. S. Jones, M. M. Marinak, J. L. Milovich, J. L. Peterson, H. F. Robey, J. D. Salmonson, V. A. Smalyuk, and C. R. Weber, "A Survey Of Pulse Shape Options For a Revised Plastic Ablator Ignition Design," Phys. Plasmas **21**, 112705 (2014)

23) J. L. Kline, K. Widmann, A. Warrick, R. E. Olson, C. A. Thomas, A. S. Moore, L. J. Suter, O. L. Landen, D. Callahan, S. Azevedo, J. Liebman, S. H. Glenzer, A. Conder, S. N. Dixit, P. Torres, V. Tran, E.L. Dewald, J. Kamperschroer, J. L. Atherton, R. Beeler, L. Berzins, J. Celeste, C. Haynam, W. Hsing, D. Larson, D. B. J. MacGowan, D. Hinkel, D. Kalantar, R. Kauffman, J. Kilkenny, N. Meezan, M. D. Rosen, M. Schneider, E. A. Williams, S. Vernon, R. J. Wallace, B. Van Wonterghem, B. K. Young, "The first measurements of soft x-ray flux from ignition scale Hohlraums at the National Ignition Facility using DANTE (invited)" Rev. Sci. Instrum., **81** (10), 10E321, 2010.

24) E. L. DeWald, K. M. Campbell, R. E. Turner, J. P. Holder, O. L. Landen, S. H. Glenzer, R. L. Kauffman, L. J. Suter, M. Landon, M. Rhodes, D. Lee, "Dante soft x-ray power diagnostic for National Ignition Facility **,"** Rev. Sci. Instrum. **75** 3759 (2004).

25) P. M. Celliers, D. K. Bradley, G. W. Collins, D. G. Hicks, T. R. Boehly, and W. J. Armstrong, "Line-imaging velocimeter for shock diagnostics at the OMEGA laser facility," Rev. Sci. Instrum. **75**, 4916 (2004).

26) L. M. Barker and R. E. Hollenbach, "Laser interferometer for measuring high velocities of any reflecting surface," J. Appl. Phys. 43, 4669 (1972).

27) P. M. Celliers, G.W. Collins, L. B. Da Silva, D. M. Gold, R. Cauble, R. J. Wallace, M. E. Foord, and B. A. Hammel, "Shock-Induced Transformation of Liquid Deuterium into a Metallic Fluid," Phys. Rev. Lett. 84, 5564 (2000).

28) M. M. Marinak, G. D. Kerbel, N. A. Gentile, O. Jones, D. Munro, S. Pollaine, T. R. Dittrich, and S. W. Haan, "Three-dimensional HYDRA simulations of National Ignition Facility targets," Physics of Plasmas 8, 2275 (2001).

29) K. Eidmann, I. B. Földes, Th. Löwer, J. Massen, R. Sigel, G. D. Tsakiris, S. Witkowski, H. Nishimura, Y. Kato, T. Endo, H. Shiraga, M. Takagi, and S. Nakai, "Radiative heating of low-Z solid foils by laser-generated x rays," Phys. Rev. E 52, 6703 (1995).

30) N. B. Meezan, A. J. MacKinnon, D. G. Hicks, E. L. Dewald, R. Tommasini, S. Le Pape, T. Döppner, T. Ma, D. R. Farley, D. H. Kalantar, P. Di Nicola, D. A. Callahan, H. F. Robey, C. A. Thomas, S. T. Prisbrey, O. S. Jones, J. L. Milovich, D. S. Clark, D. C. Eder, M. B. Schneider, K. Widmann, J. A. Koch, J. D. Salmonson, Y. P. Opachich, L. R. Benedetti, S. F. Khan, A. G. MacPhee, S. M. Glenn, D. K. Bradley, E. G. Dzenitis, B. R. Nathan, J. J. Kroll, A. V. Hamza, S. N. Dixit, L. J. Atherton, O. L. Landen, S. H. Glenzer, W. W. Hsing, L. J. Suter, M. J. Edwards, B. J. MacGowan, E. I. Moses, R. E. Olson, J. L. Kline, G. A. Kyrala, A. S. Moore, J. D. Kilkenny, A. Nikroo, K. Moreno, and D. E. Hoover, "X-ray driven implosions at ignition relevant velocities on the National Ignition Facility," Physics of Plasmas **20**, 056311 (2013).

31) John Lindl, "Development of the indirect-drive approach to inertial confinement fusion and the target physics basis for ignition and gain**,**" Phys. Plasmas **2**, 3933 (1995)

32) M. A. Barrios, T. R. Boehly, D. G. Hicks, D. E. Fratanduono, J. H. Eggert, G. W. Collins, and D. D. Meyerhofer, "Precision equation-of-state measurements on National Ignition Facility ablator materials from 1 to 12 Mbar using laser-driven shock waves," J. Appl. Phys. **111**, 093515 (2012).

33) S. W. Haan, J. D. Lindl, D. A. Callahan, D. S. Clark, J. D. Salmonson, B. A. Hammel, L. J. Atherton, R. C. Cook, M. J. Edwards, S. Glenzer, A. V. Hamza, S. P. Hatchett, M. C. Herrmann, D. E. Hinkel, D. D. Ho, H. Huang, O. S. Jones, J. Kline, G. Kyrala, O. L. Landen, B. J. MacGowan, M. M. Marinak, D. D. Meyerhofer, J. L. Milovich, K. A. Moreno, E. I. Moses, D. H. Munro, A. Nikroo, R. E. Olson, K. Peterson, S. M. Pollaine, J. E. Ralph, H. F. Robey, B. K.

Spears, P. T. Springer, L. J. Suter, C. A. Thomas, R. P. Town, R. Vesey, S. V. Weber, H. L.Wilkens, and D. C Wilson, "Point design targets, specifications, and requirements for the 2010 ignition campaign on the National Ignition Facility," Physics of Plasmas **18**, 051001 (2011).

34) Gerald I. Kerley, "Equations of State for Hydrogen and Deuterium," *Sandia National Laboratories Report SAND* 2003-3613 (2003).

35) Sebastien Hamel, Lorin X. Benedict, Peter M. Celliers, M. A. Barrios, T. R. Boehly, G. W. Collins, Tilo Do ppner, J. H. Eggert, D. R. Farley, D. G. Hicks, J. L. Kline, A. Lazicki, S. LePape, A. J. Mackinnon, J. D. Moody, H. F. Robey, Eric Schwegler, and Philip A. Sterne, "Equation of state of CH1.36: First-principles molecular dynamics simulations and shock-and-release wave speed measurements," Physical Review B **86**, 094113 (2012).

36) P. Clark Souers, *Hydrogen Properties for Fusion Energy* (University of California Press, Berkeley, 1986), p. 62.

# FIGURE CAPTIONS

Figure 1 Laser pulse shapes used to drive the hohlraums in each of the experiments. The LF pulse shape is represented by the dashed black line, the AS LF 1 pulse by the purple line, the AS LF 2 pulse by the blue line, the HF AS pulse by the green line and the HF pulse by the dashed red line. Fig. 1a shows the entire pulse shape record and Fig. 1b shows only the foot of the pulses, the picket and trough.

Figure 2 Hohlraum radiation temperature profiles as measured by and unfolded from the Dante diagnostic. The radiation temperature driven by the LF pulse shape is represented by the dashed black line, the AS LF 1 pulse by the purple line, the AS LF 2 pulse by the blue line, the HF AS pulse by the green line and the HF pulse by the dashed red line.

Figure 3 Fig, 3a shows the shock velocity temporal profiles as measured by and unfolded from the VISAR diagnostic in each of the experiments. The shock velocity driven by the LF pulse shape is represented by the dashed black line, the AS LF 1 pulse by the purple line, the AS LF 2 pulse by the blue line, the HF AS pulse by the green line and the HF pulse by the dashed red line. Fig. 3b represents a HYDRA simulation of a DT experiment with D2 liquid replacing the DT ice and DT gas and it shows the position of the leading shock as a function of time in red. This leading shock position represents the surface from which the VISAR is reflected.

Figure 4 Simulated shock pressure profiles in a DT ignition experiment using the Hydra code. The shock pressure driven by the LF pulse shape is represented by the dashed black line, the AS LF 1 pulse by the purple line, the AS LF 2 pulse by the blue line, the HF AS pulse by the green line and the HF pulse by the dashed red line.

Figure 5 Fig. 5a represents the simulated fuel adiabat profiles vs. time for each of the five laser pulse shapes. The fuel adiabat is represented by the dashed black line, the AS LF 1 pulse by the purple line, the AS LF 2 pulse by the blue line, the HF AS pulse by the green line and the HF pulse by the dashed red line. Fig. 5b represents a simulation of the fuel adiabat where the adiabat is quantified as the average over the central 20% of the fuel layer. This has the feature of clearly indicating the separate contributions of the various shocks to the adiabat. The same color convention as used in Fig. 5a is used in Fig. 5b.

Figure 6 Shock velocity in the GDP vs. shock velocity in the liquid deuterium for each of the five laser pulse shapes. The experimental data points for each of the five laser pulse shapes are listed and follow the same color convention as the previous graphs. The solid black line shows the release curve generated from the GDP (LEOS 5400) and liquid deuterium (LEOS 1014) equation of state tables.

Figure 7 The Hugoniot and the isentropes for each of the five laser pulses along with the cold curve. Figure 7a represents a large pressure-density space with Fig. 7b displaying a more limited pressure-density region where the adiabat is determined. The curves follow the same color convention as the previous graphs with the Hugoniot represented by the black line and the cold curve by the gray line.

# FIGURES

KL Baker

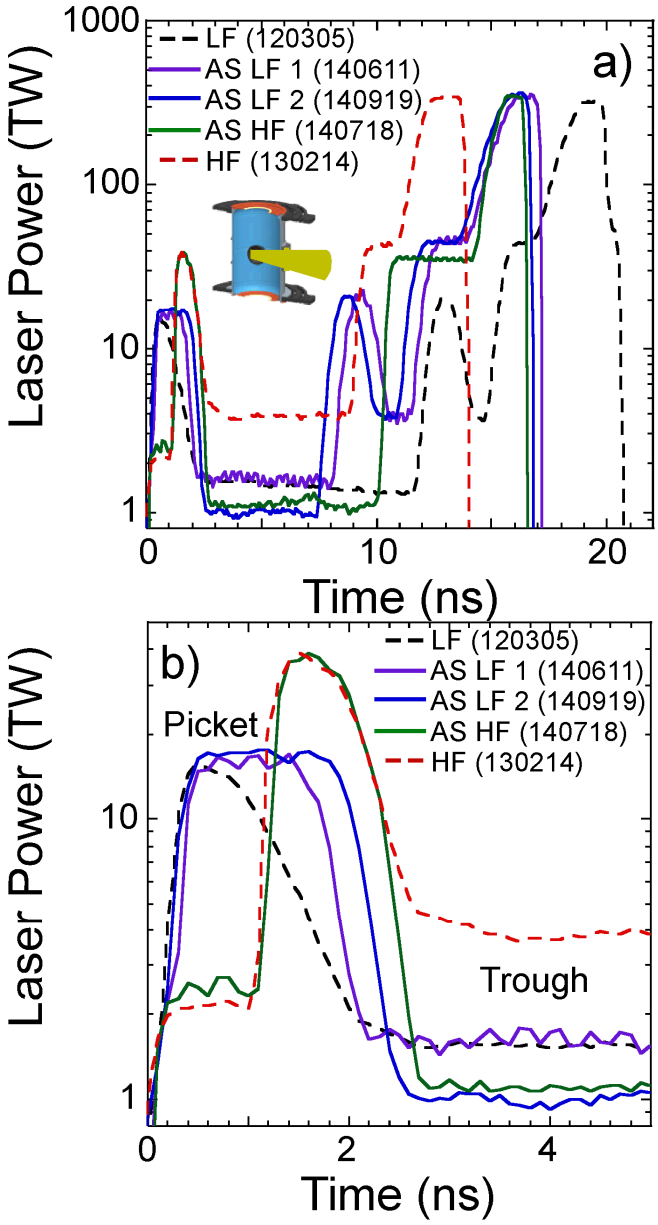


Figure 1

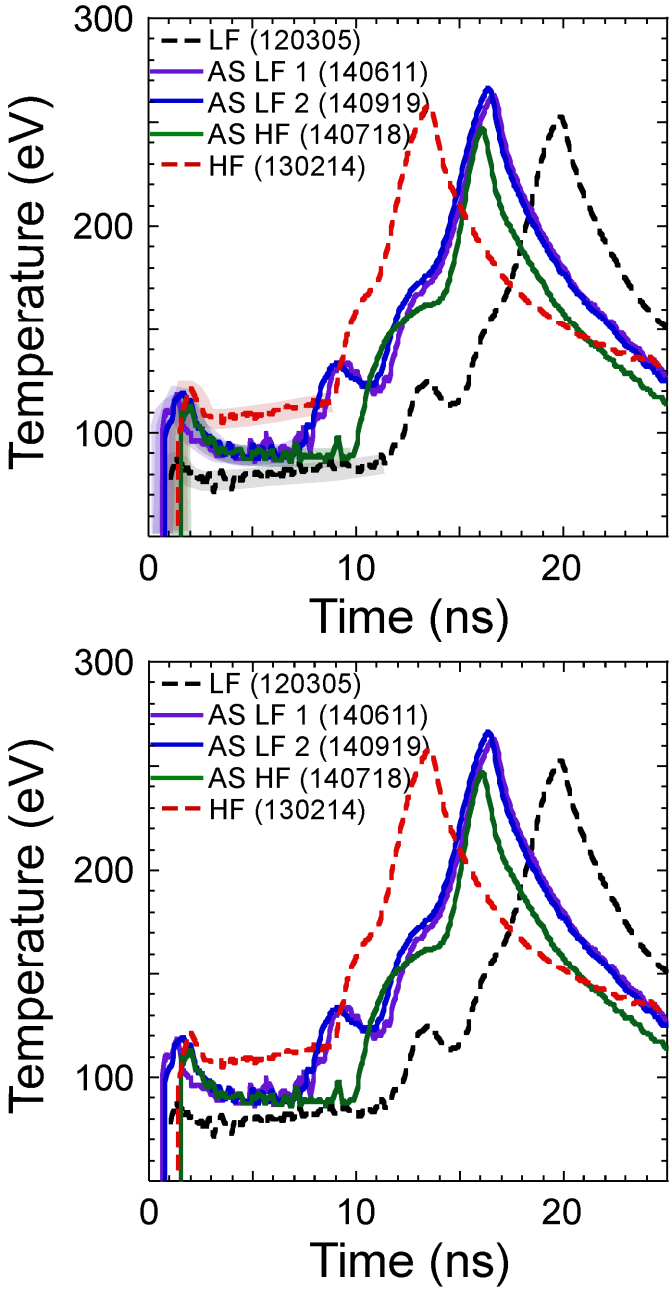
300
200
100
Temperature (eV)
LF (120305)
AS LF 1 (140611)
AS LF 2 (140919)
AS HF (140718)
HF (130214)
0
10
20
Time (ns)
300
200
100
Temperature (eV)
LF (120305)
AS LF 1 (140611)
AS LF 2 (140919)
AS HF (140718)
HF (130214)
0
10
20
Time (ns)

Figure 2

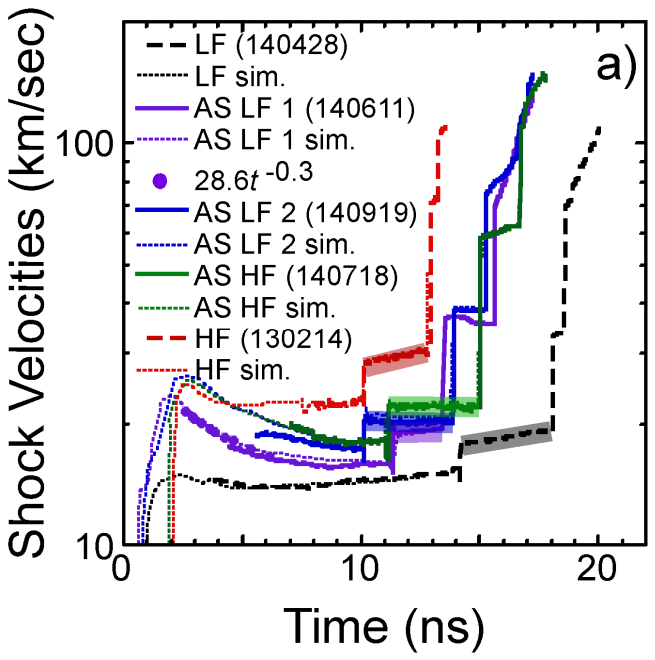


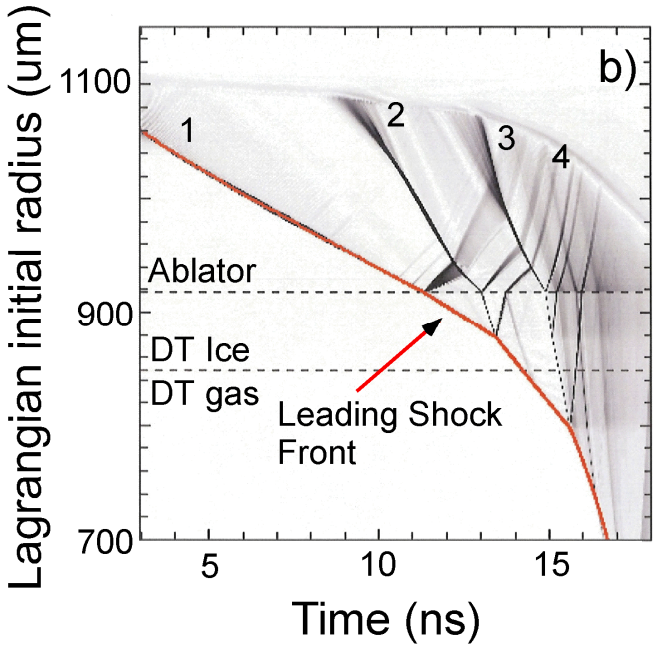


Figure 3

KL Baker

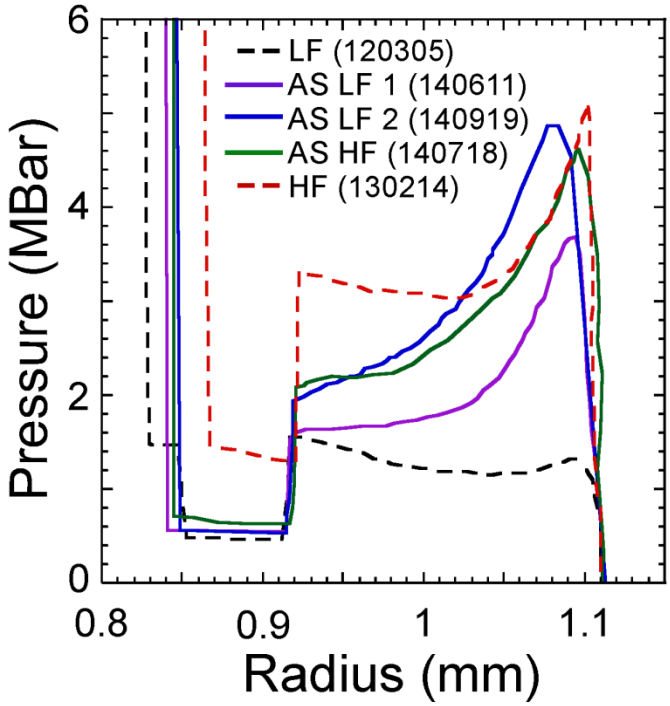
LF (120305)
AS LF 1 (140611)
AS LF 2 (140919)
AS HF (140718)
HF (130214)
Pressure (MBar)
Radius (mm)
0
2
4
6
0.8
0.9
1
1.1

Figure 4

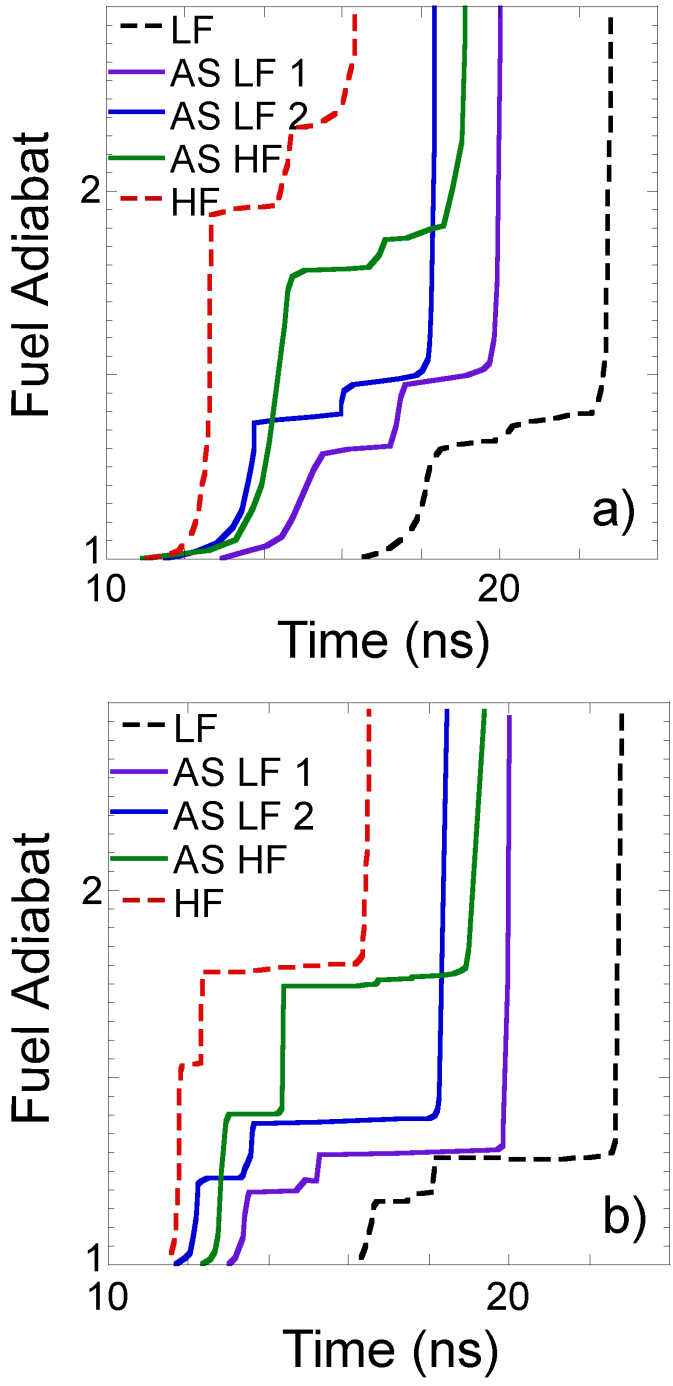
LF
AS LF 1
AS LF 2
AS HF
HF
Fuel Adiabat
2
1
10
20
Time (ns)
a)
LF
AS LF 1
AS LF 2
AS HF
HF
Fuel Adiabat
2
1
10
20
Time (ns)
b)

Figure 5

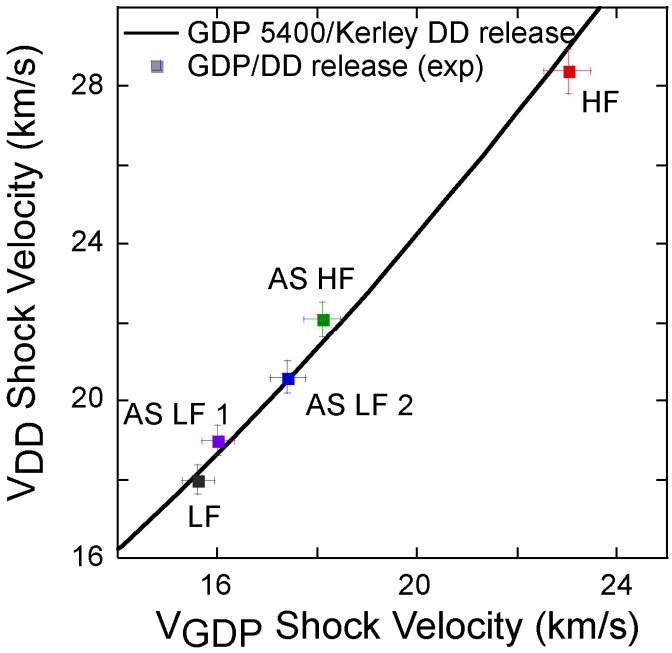
GDP 5400/Kerley DD release
GDP/DD release (exp)
HF
AS HF
AS LF 2
AS LF 1
LF
28
24
20
16
16
20
24
VDD Shock Velocity (km/s)
VGDP Shock Velocity (km/s)

Figure 6

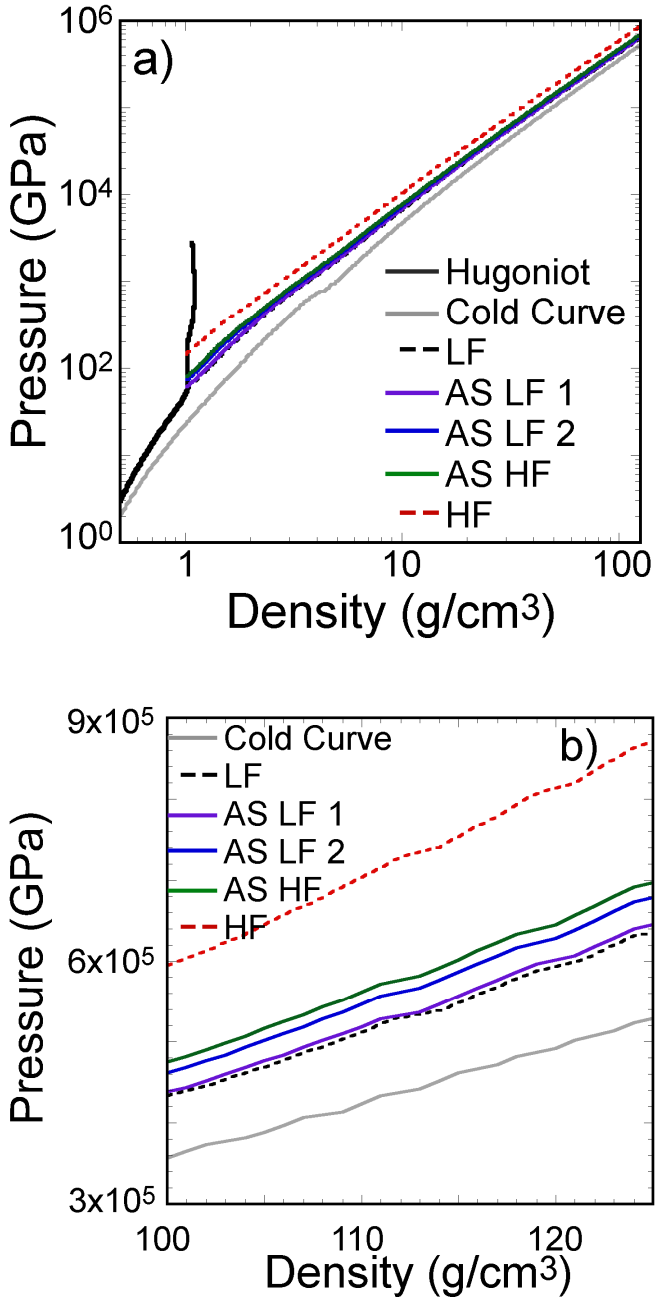
a)
Pressure (GPa)
Density (g/cm3)
Hugoniot
Cold Curve
LF
AS LF 1
AS LF 2
AS HF
HF
b)
Pressure (GPa)
Density (g/cm3)
Cold Curve
LF
AS LF 1
AS LF 2
AS HF
HF

Figure 7

| | LF | AS LF1 | AS LF2 | AS HF | HF |
|---|---|---|---|---|---|
| $V_{GDP\text{-}picket}$ (km/s) sim. | 14.9 | 23.48 | 26.4 | 25.7 | 25.06 |
| $T_{r\text{-}picket}$ (eV) exp. | 88. | 119 | 120 | 113 | 122 |
| $T_{r\text{-}trough}$ (eV) exp. | 87 | 92 | 92 | 90 | 115 |
| $V_{GDP\text{-}trough}$ (km/s) mod. | 14.66 | 16.25 | 18.05 | 19.15 | 23.03 |
| $V_{GDP\text{-}trough}$ (km/s) exp. | 15.60 | 16.00 | 17.40 | 18.10 | 23.00 |
| $\%V_{GDP\text{-}trough}$ diff. | 6.0 | 1.6 | 3.7 | 5.8 | 0.1 |

Table 1

| | LF | AS LF1 | AS LF2 | AS HF | HF |
|---|---|---|---|---|---|
| $V_{GDP}$ (km/s) exp. | 15.60 | 16.00 | 17.40 | 18.10 | 23.00 |
| $V_{DD}$ (km/s) exp. | 18.00 | 19.00 | 20.60 | 22.10 | 28.40 |
| $V_{DD}$ (km/s) model | 18.16 | 18.66 | 20.52 | 21.49 | 28.96 |
| $P_{DD}$ (GPa) model | 43.40 | 45.95 | 55.75 | 61.16 | 110.25 |
| $V_{DT}$ (km/s) model | 17.26 | 17.75 | 19.54 | 20.47 | 27.52 |
| $P_{DT}$ (GPa) model | 56.73 | 60.09 | 73.01 | 80.11 | 144.21 |
| DD adiabat model | 1.19 | 1.20 | 1.26 | 1.30 | 1.63 |
| DT adiabat model | 1.20 | 1.22 | 1.28 | 1.32 | 1.64 |
| DD adiabat simulation | 1.17 | 1.2 | 1.23 | 1.41 | 1.54 |
| % adiabat diff. | 1.7 | 0 | 2.4 | 7.8 | 5.8 |

Table 2